Journal of Medicinal Chemistry Article

J. Med. Chem. **2009,** *52,* 7003–7013 **7003**
DOI: 10.1021/jm9005077

Binding Ensemble Profiling with Photoaffinity Labeling (BEProFL) Approach: Mapping the Binding Poses of HDAC8 Inhibitors

Bai He,[†] Subash Velaparthi,[†] Gilles Pieffet,[†] Chris Pennington,[†,§] Aruna Mahesh,[‡] Denise L. Holzle,[‡] Michael Brunsteiner,[†] Richard van Breemen,[†] Sylvie Y. Blond,[‡,∥] and Pavel A. Petukhov*,[†]

[†]*Department of Medicinal Chemistry and Pharmacognosy, College of Pharmacy, University of Illinois at Chicago, 833 South Wood Street, Chicago, Illinois 60612, and* [‡]*Center for Pharmaceutical Biotechnology, University of Illinois at Chicago, 900 South Ashland, Chicago, Illinois 60612.* [§]*Present address: Abbott Laboratories GPRD, Process Analytical Chemistry, 1401 Sheridan Road, North Chicago, Illinois 60064.* [∥] *Alternative address: Institut de Génétique Moléculaire, INSERM/University Denis Diderot Paris 7, UMRS-940, 27 Rue Juliette Dodu, 75010 Paris, France.*

Received April 21, 2009

A **b**inding **e**nsemble **pro**filing with (**f**)photoaffinity **l**abeling (BEProFL) approach that utilizes photolabeling of HDAC8 with a probe containing a UV-activated aromatic azide, mapping of the covalent modifications by liquid chromatography−tandem mass spectrometry, and a computational method to characterize the multiple binding poses of the probe is described. By use of the BEProFL approach, two distinct binding poses of the HDAC8 probe were identified. The data also suggest that an "upside-down" pose with the surface binding group of the probe bound in an alternative pocket near the catalytic site may contribute to the binding.

Introduction

Histone deacetylases (HDACs[a]) comprise a family of enzymes that regulate chromatin remodeling, gene transcription, and activity of partner proteins. They control critical cellular processes, including cell growth, cell cycle regulation, DNA repair, differentiation, proliferation, and apoptosis.[1] Chemical inhibitors of HDACs (Figure 1) have been shown to inhibit tumor cell growth and induce differentiation and cell death.[2] SAHA (**1**, Figure 1) has been recently approved by FDA for use against cutaneous T-cell lymphoma. The HDACs can be divided into four classes based on structure, sequence homology, and domain organization.[3] It is hypothesized that depending on isoform selectivity HDAC ligands can be either cytotoxic or neuroprotective.[4] The development of isoform-selective HDAC inhibitors would be a significant step in reducing off-target effects of HDAC-based therapeutics.

One of the key challenges in designing isoform-selective HDAC inhibitors is a poor understanding of the binding modes (poses) available to the highly solvent exposed surface binding group (SBG) of HDAC inhibitors targeting the grooves and ridges on the protein surface directly adjacent to the catalytic well of HDACs (Figure 2). It has been hypothesized by us in our preliminary experiments and a recent publication by Wiest and colleagues[5] that the SBG groups may have more than one preferred position on the surface and each of them contributes to the overall binding affinity. Although the available HDAC X-ray data provide information on structure of proteins and binding of ligands, its use is limited because of high solvent exposure of the SBG of the ligands and additional copies of the same protein in the

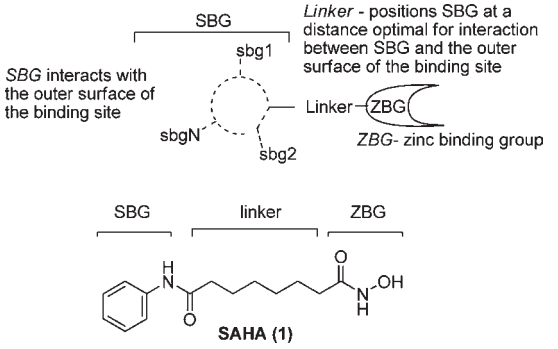

Figure 1. General structure of HDAC inhibitors.

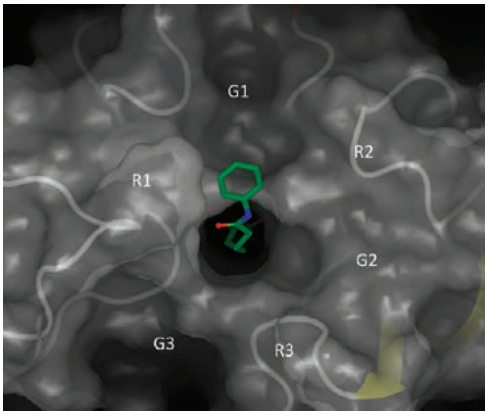

Figure 2. Description of the grooves (G1−G3) and ridges (R1−R3) formed by the protein surface of HDAC8 (PDB 1T69).

*To whom correspondence should be addressed. Phone: 312-996-4174. Fax: 312-996-7107. E-mail: pap4@uic.edu.

[a] Abbreviations: HDAC, histone deacetylase; BEProFL, **b**inding **e**nsemble **pro**filing with (**f**)photoaffinity **l**abeling; BT, biotin tag; ArN_3, aromatic azide group; $AlkN_3$, aliphatic azide group; ZBG, zinc binding group; SBG, surface binding group; linker, a portion of the molecule connecting the zinc binding group and surface binding group; SAHA, suberoylanilide hydroxamic acid; TSA, trichostatin A.

Published on Web 11/03/2009

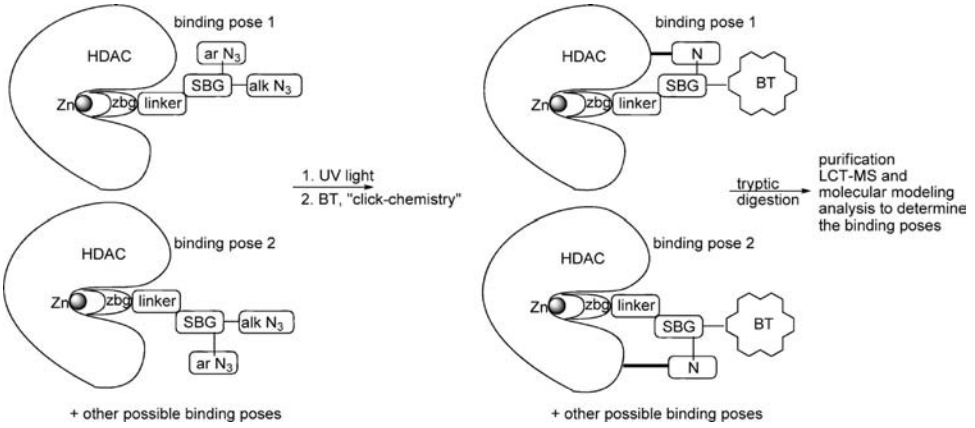

Figure 3. Application of photoaffinity probes for detection of binding poses of an HDAC ligand.

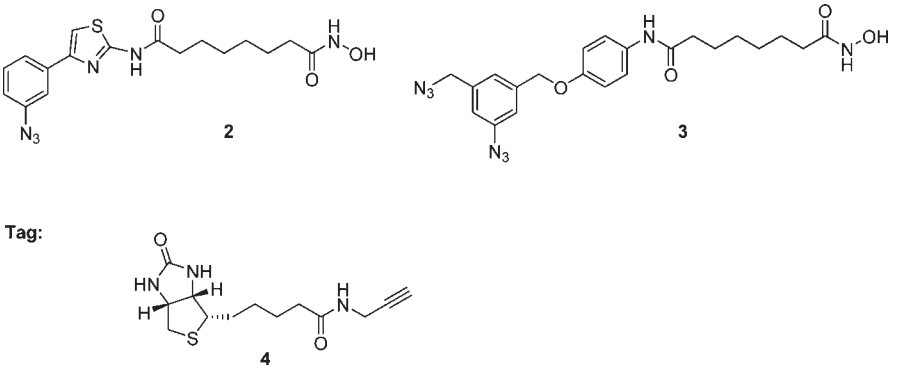

Figure 4. Chemical structures of the probes **2** and **3** and the biotin tag **4**.

crystallographic cell that interfere with the binding of the cocrystallized ligands.

Photoaffinity labeling is a strategy offering methods for the identification of drug target proteins of biologically active compounds and mapping their binding sites.[6−8] Among several photosensitive groups, arylazide is perhaps one of the most widely used because of its universality, reactivity, and relative simplicity in implementation.[6] One of the recent advances in the photoaffinity labeling probe development is application of "click-chemistry" and bioorthogonal probes for activity-based proteomics profiling by Cravatt et al.[9−15] and its recent modification by Suzuki et al.[16−18] This latter study is based on a concept in which a bifunctional ligand is connected to a target protein by activation of a photoreactive group, such as an aromatic azido or 3-trifluoromethyl-3*H*-diazirin-3-yl group, and identification of the ligand product is achieved by anchoring a detectable tag to an alkylazido moiety, which survives photolysis, using the Staudinger−Bertozzi ligation.[19−24] A similar approach was recently utilized to discover a new binding site in HIV-1 integrase.[25] In this case a different photoactivated moiety, benzophenone, facilitated by mass spectrometry and docking analysis was used to determine the exact ligand binding position. The recent study by Cravatt et al.[15] presents a novel proteomics probe for histone deacetylases and is intended to discover new proteins interacting with the histone deacetylases. It does not address, however, the problem of multiple binding poses of HDAC inhibitors.

Here we introduced for the first time the use of diazide-based photoaffinity labeling probes, liquid chromatography−tandem mass spectrometry, and molecular dynamics simulations to map the ensemble of the poses of HDAC8 inhibitors upon binding (Figure 3) or BEProFL (**b**inding **e**nsemble **pro**filing with (**f**)photoaffinity **l**abeling).

Chemistry and Analyses

Synthesis. The synthesis of probes **2** and **3** (Figure 4) is outlined in Schemes 1 and 2. Commercially available subericacid monomethyl ester **5** was coupled with 4-(3-nitrophenyl)thiazol-2-ylamine in the presence of pyridine and $POCl_3$ to give ester **6**.[26] The nitro group of ester **6** was reduced resulting in amine **7** that was converted to azide **8** by diazotization and nucleophilic substitution with sodium azide. Further treatment of **8** with hydroxylamine resulted in hydroxamic acid **2**. The condensation of **5** with an equivalent amount of 4-benzyloxyaniline in the presence of $POCl_3$ and pyridine gave amide **9**. The benzylhydroxy group of amide **9** was deprotected by catalytic hydrogenation and coupled with mesylate **12**,[27] resulting in diazide **11** that was then converted to the corresponding hydroxamic acid **3** in a 40% yield. BT **4** was synthesized following the procedure described earlier.[28]

HDAC Activity Assay. The inhibition of HDAC8 was measured as recommended by the supplier BIOMOL International using the fluorescent acetylated HDAC substrate Fluor de Lys (BIOMOL, KI178) and commercially available recombinant human HDAC8 (BIOMOL). The activity data are summarized in Table 1.

Photolabeling and Visualization of Probes. The probes **2** and **3** or probe **3**−SAHA mixture (in the competition experiment) were incubated with the HDAC8 protein, exposed to 254 nM UV light 3 × 1 min with 1 min resting. In the

Scheme 1. Synthesis of Probe **2**[a]

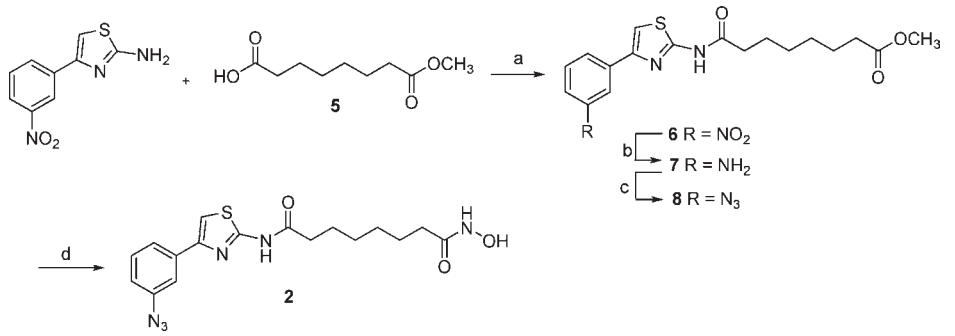

[a] Reagents and conditions: (a) $POCl_3$, pyridine, 12 h, room temp, 76%; (b) H_2, Pd−C, EtOH, AcOH, 50 °C, 2 h, 80%; (c) $NaNO_2$, $AcOH/H_2O$ (9:1), 0 °C, 3 min, then NaN_3, 0 °C, 30 min, 73%; (d) $NH_2OH \cdot HCl$, KOH, MeOH, 4 h, 0 °C to room temp, 28%.

Scheme 2. Synthesis of Probe **3**[a]

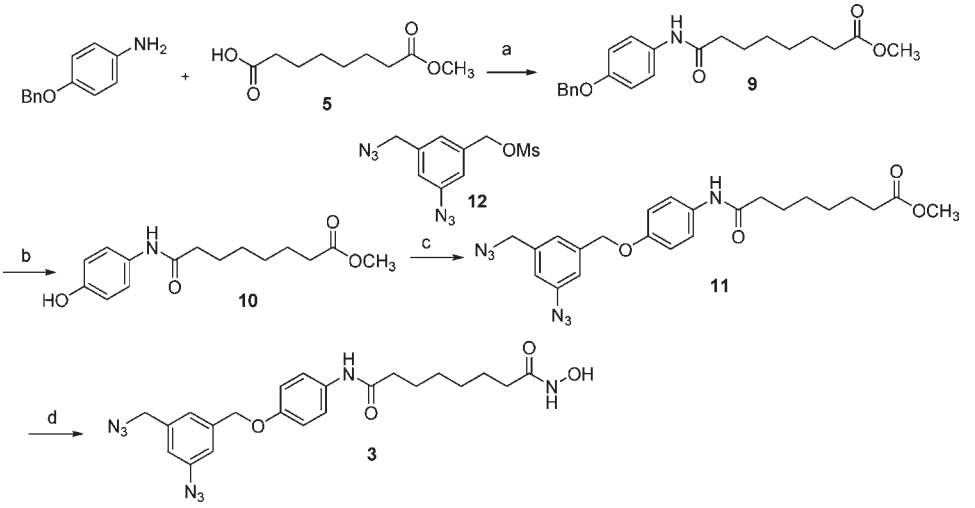

[a] Reagents and conditions: (a) $POCl_3$, pyridine, 12 h, room temp, 61%; (b) H_2, Pd−C, MeOH, room temp, 5 h, 81%; (c) K_2CO_3, acetone, 12 h, 66%; (d) $NH_2OH \cdot HCl$, KOH, MeOH, 4 h, 0 °C to room temp, 40%.

Table 1. IC_{50} and K_I Values of Inhibition of HDAC8 with SAHA and Probes **2** and **3**

	HDAC8	
compd	IC_{50} (μM)	K_i (μM)
SAHA	0.44 ± 0.021	0.396
2	2.71 ± 0.14	2.43
3	7.34 ± 0.22	6.59

case of **3**, BT **4** was attached to HDAC8−**3** adduct using [3 + 2]-cycloligation catalyzed by TBTA and Cu(I) produced in situ from $CuSO_4$ with TCEP. The tagged HDAC8 protein was visualized with Western blotting. The procedures were in general similar to those recently described by Cravatt et al.[15] and Suzuki et al.[16−18] The results are shown in Figure 5.

MALDI-ToF MS Analysis of Intact HDAC8 Protein. The four HDAC8 samples (three of them were treated with **2** at different concentrations) were purified and subjected to MALDI-ToF MS positive ion analysis. The results are shown in Table 2.

Tryptic Digestion and 1-D LC−MS/MS Analysis. HDAC8 protein was incubated with the photoaffinity probe **3**, exposed to UV light to form HDAC8−**3** covalent adduct, and tagged with BT **4**. Next, the modified protein was purified using avidin−agarose chromatography. Unmodified HDAC8 was used as a negative control. To facilitate the analysis of the modified protein, tryptic digestion was carried out followed by mass spectrometric liquid chromatography−tandem mass spectrometry (LC−MS/MS) and proteomics database analyses using SEQUEST proteomics software. Two proteomics data sets were generated; one used an accurate mass peptide mass tolerance of 5 ppm between the theoretical and measured peptide masses, and the second data set used a mass tolerance of 10 ppm. It should be noted that both 5 and 10 ppm are considered accurate mass measurements. The results are provided in Table 3 and Figures 6−8.

Molecular Dynamics Simulations. Molecular Dynamics Simulations of SAHA and ligand **3** in complex with HDAC8 were performed using the GROMACS software package (version 3.3.1)[29−32] and the Amber03 force field[33] as ported to GROMACS.[34] Ligands were parametrized using the general Amber force field (GAFF)[35,36] augmented with custom azide parameters[37]and AM1BCC charges.[38,39] The structure of HDAC8 and the starting conformation of SAHA were taken from PDB 1T69. The starting structures for **3** were obtained from the docking with Gold 3.2.[40] Root mean square deviation (rmsd) matrices of the ligands were built for each simulation trajectory by calculating the rmsd of each structure of the ligand with all other structures of the same ligand in the trajectory. All protein structures in the trajectory were aligned using the least-squares fitting of the protein backbone. The final rmsd calculations of the ligands

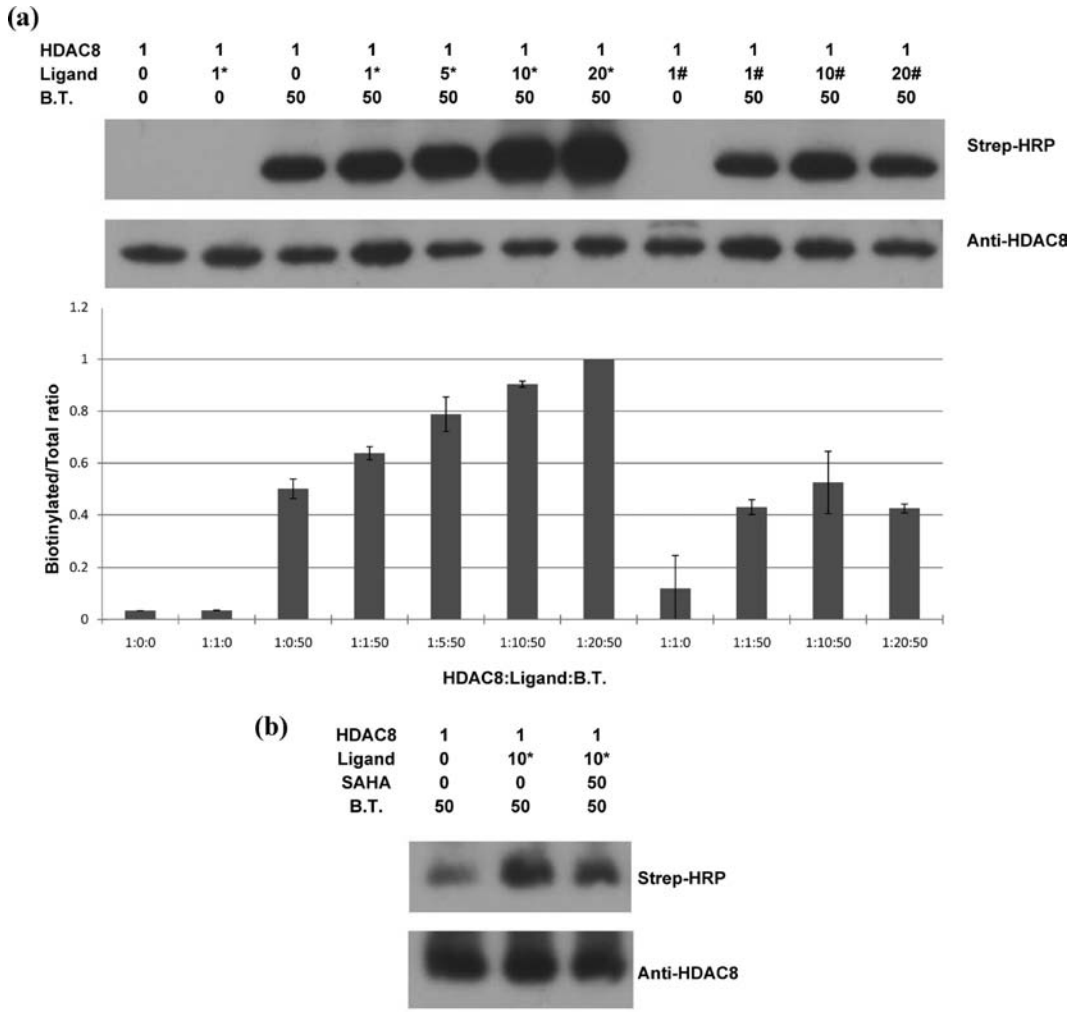

Figure 5. Characterization of biotinylated HDAC proteins and total HDAC proteins. (a) Western blot analyses of probe **2** (labeled as #) and probe **3** (labeled as ∗) binding to HDAC8 probed by strep-HRP and anti-HDAC8 antibodies. All the numbers stand for the concentration in μM. (b) Same as for part a. Competition of probe **3** with SAHA.

Table 2. MALDI MS of Intact HDAC8 and Treated with **2**

sample	*N*	av MW (Da) $[M + H]^+$	std dev	mass shift, Δ CTRL
HDAC8 CTRL	6.0	45 620	57.5	0.0
HDAC8 (1:1)	6.0	45 624	41.3	4.0
HDAC8 (1:5)	6.0	45 733	37.1	113.5
HDAC8 (1:10)	4.0	45 877	37.1	256.8

were performed on their heavy atoms using the atoms corresponding to the scaffold of SAHA. The results of the rmsd calculations are given in Supporting Information together with the analysis of the distances between the SBGs of SAHA and ligand **3** and representative amino acids in G1−G3. The most representative binding poses are shown in Figure 9.

Results and Discussion

A general idea for capturing the binding poses of the HDAC probe using BEProFL approach is outlined in Figure 3. Among other reactive groups typically used for covalent modification of the protein we selected an aromatic azide because (1) it is hydrophobic and therefore is likely to stay near the protein surface, minimizing the reaction with the solvent and maximizing the amount of the covalently modified protein, and (2) upon UV photoactivation it generates a nitrene moiety known to be very reactive and nonspecific, which is expected to be essential for capturing a "snapshot" of the bound probe close to where this reactive moiety was generated. In addition there are several critical requirements for photoaffinity probes in general. First, the probes should exhibit a respectable level of HDAC binding to maximize the yield of the modified HDAC protein. Second, the procedures for UV-activated cross-linking should be efficient enough so that the UV damage of the protein is minimized while the yield of the cross-linked adduct is maximized. Third, the attachment procedure of the biotin probe should be fast and efficient to minimize possible aggregation and precipitation of the protein.

The probes used in this study were designed to mimic the scaffold of SAHA (**1**) and a phenylthiazole-based HDAC inhibitor.[41] The synthesis of probes **2** and **3** is shown in Schemes 1 and 2. It was found that probe **2** is 6.1-fold and probe **3** is 16.6-fold less active in inhibiting HDAC8 compared to SAHA (Table 1). The moderate HDAC8 activity of the ligands with this scaffold is consistent with other reports.[42] The decrease in activity of the probes is not surprising, since introduction of the azide moieties in probes **2** and **3** increased the lipophilic nature of the solvent exposed SBGs.

The success of the procedure shown in Figure 3 depends on the ability of the probes to modify the protein rather than the solvent surrounding the ligand and the protein. Since the SBG

Table 3. Summary of Identified HDAC8 Peptides Modified with Probe **3**−BT **4** Adduct

entry no.	peptide[a]	sequence (AA nos.)	$[M + H]^+$	m/z	charge state (z)	no. of mods	mass tolerance (ppm)
1	IPKRASM*VHSLIEAYALHKQM*R	034−055	3330.72571	1109.57524	3	1	5
2	RASMVHSLIEAYALHKQM*RIVKPK	037−060	3541.88969	886.22242	4	1	10
3	ASM*VHSLIEAYALHKQMRIVKPK	038−060	4105.10938	1367.70313	3	2	5
4	ASM*VHSLIEAYALHKQMRIVKPK	038−060	4105.10938	1367.70313	3	2	5
5	QM*RIVKPK.	053−060	1734.93338	867.96669	2	1	10
6	VAINWSGGWHHAKK	133−145	2901.37544	1450.18772	2	2	5
7	DEASGFCYLNDAVLGILRLRRKFER	147−171	3660.86731	609.31122	6	1	5
8	GRYYSVNVPIQDGIQDEK	222−239	2800.35061	934.11687	3	1	10
9	YYQICESVLKEVYQAFNPK	240−258	3041.46828	1521.23414	2	1	10
10	AVVLQLGADTIAGDPMCSFNMTPVGIGK	259−286	4244.03997	1060.25999	4	2	5
11	AVVLQLGADTIAGDPMCSFNMTPVGIGK	259−286	4244.03997	849.60799	5	2	10

[a] The asterisk (*) indicates an oxidized methionine. The underlined residues correspond to the region of the HDAC8 protein where modification by probe **3** occurred.

of HDAC inhibitors is highly solvent exposed, there was a chance that the aromatic azide moiety would not be able to reach the protein surface and instead would prefer to react with the solvent.

As the first step, we confirmed that an aromatic azide group can indeed be used to covalently attach the probes to the HDAC8 protein by detecting a mass shift in a MALDI MS experiment. The results of the MALDI MS analysis are summarized in Table 2. The average mass of the untreated HDAC8 protein was 45 620 Da. After incubation with ligand **2**, the mass of the HDAC8 protein increased in dose-dependent manner. A maximum mass shift of 256.8 Da was observed at an enzyme to reagent ratio of 1:10. As the amount of protein modified approaches 100%, the observed average mass shift would be expected to approach the mass of the reagent (360 Da). We attribute the relatively high concentration of probe **2** needed to its relatively poor potency against HDAC8 and high solvent exposure of the SBG. The results of the MALDI-MS analysis of the intact protein supported the conclusion that the protein was successfully modified by the UV activated nitrene group generated from the probe **2**, and we moved to the next stage, cross-linking followed by attachment of BT **4** to the alkyl azide moiety of probe **3**.

To evaluate the selectivity of photolabeling in vitro, purified recombinant HDAC8 was incubated with various concentrations of ligands **2** and **3**. The conditions for UV cross-linking were optimized to increase the signal-to-noise ratio. We found that in case of HDAC8 3 × 1 min exposure to UV light with 1 min rest gives the best signal-to-noise ratio. The "click-chemistry" conditions with catalysis by Cu(I) generated in situ were successfully used to attach BT **4** to the adduct between HDAC8 and probe **3**. In our preliminary studies we also tried the Staudinger−Bertozzi ligation[19−24] as an attachment procedure of the biotin tag and determined that the "click-chemistry" approach is much faster and gives better yield as determined by Western blotting. This is consistent with the observation made by Cravatt et al.[9]

As expected, the amount of biotinylated HDAC increases in a concentration-dependent manner in the presence of ligand **3** but not with ligand **2** (Figure 5a) that lacks the alkyl azide group designed to bind the biotin tag; only nonspecific, background level signals are observed. A comparison of the background levels observed in lanes 3 and 9−11 shows that the background levels of biotinylation are due to nonspecific modification of the HDAC8 protein with BT **4** and do not depend on the presence of probes **2** and **3**. It appears that the nonspecific biotinylation with BT **4** may be specific to the HDAC8 protein because in a similar experiment HDAC3 protein showed negligible levels of nonspecific biotinylation with BT **4** (data not shown). In the competition experiment shown in Figure 5b, the level of the covalent modifications with probe **3** drops by 50% when SAHA is present during the photolabeling, indicating that the cross-linking of the probe **3** to HDAC8 is likely to happen when **3** is bound at the catalytic site.

A total of 11 modified HDAC8 peptides were identified from the avidin−agarose purified HDAC8−**3**,**4** adduct based on peptide mapping using high resolution accurate mass measurement (within 10 ppm) and peptide sequencing using MS/MS (Table 3). No modified peptides were detected in the negative control using unmodified HDAC8 (data not shown). The amino acids underlined in Table 3 correspond to the residues modified by **3** based on MS/MS analysis. Because of occasional missed trypsin cleavage sites, which are common in trypsinization reactions, there are some amino acid sequence overlaps among several peptides. For example, entries 1 and 2 correspond to overlapping amino acid sequences 35−55 and 37−60, respectively. Also, because of the high reactivity of the photoaffinity ligand, several amino acid residues became modified in entries 3, 4, 6, 10, and 11 (Table 3).

Among the sites modified by probe **3** (Table 3, Figure 8a), the two nearest the binding site amino acids located on the surface of the protein were Asp^{233} and Asp^{272}. Asp^{272} maps to the R2/G1 region of HDAC8, and Asp^{233} neighbors with the R2/G2 (Figure 2). The two other areas near the binding site corresponding to His^{142}-His^{143} (entry 6, Table 3) and Ile^{135}-Asn^{136}-Trp^{137}-Ser^{138} (entry 6, Table 3) are not on the surface of the protein. Photolabeling of these residues may be explained if the binding site of HDAC8 adopts a conformation similar to that found in 1T64 X-ray structure where the second molecule of TSA is bound upside down.[43] The access to these residues in other crystal structures is blocked by loop L1 (Figure 8b) that was shown to shift its position to accommodate the second molecule of TSA. If loop L1 swings far enough, it may expose the residues in entries 1−6 for modification by the SBG of probe **3**. The other labeled peptides correspond to sites on the outer periphery of HDAC8 and were likely modified by excess unbound **3** upon activation by UV light. An analysis of these areas shows that they are either hydrophobic or close to hydrophobic areas and thus may participate in aggregation with probe **3**.

Modified Asp^{233} was contained in peptide GRYYSVNVPIQDGIQDEK (222−239), and the MS/MS spectrum of this modified peptide is shown in Figure 6. On the basis of Sequest proteomics analysis, the standard peptide fragment ions such as y_6^{1+} and a_{15}^{2+} were identified, and manual inspection of the

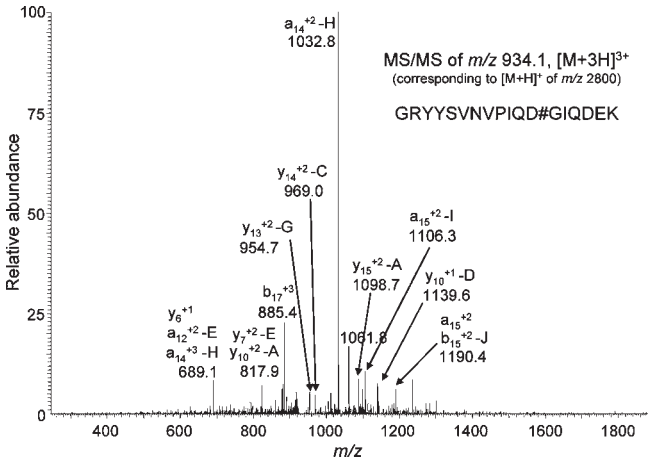

Figure 6. MS/MS spectrum of HDAC8 tryptic peptide 222−239, GRYYSVNVPIQDGIQDEK (see Table 3, entry 8), showing alkylation at Asp^{233}. The peaks are annotated using the conventional proteomics MS/MS nomenclature (e.g., y_6^{1+}). Upper case letters denote the additional side chain cleavages of ligand **3** modified by biotin tag **4** (the structures of possible fragmentation of the resulting construct are shown in Figure 7).

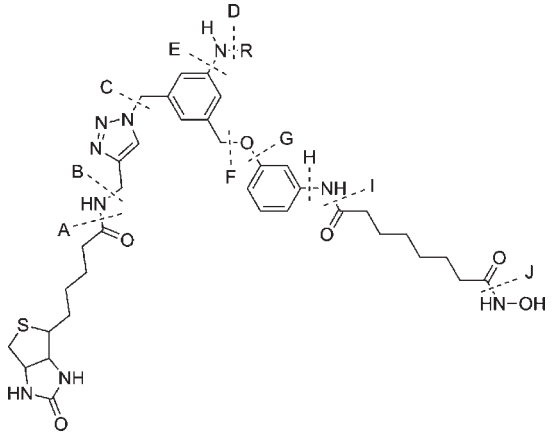

Figure 7. Structure and 10 possible bond cleavages of ligand **3** modified with biotin tag **4**. Bond cleavages are labeled A−J, and R denotes the amino acid side chain.

data was used to identify additional fragment ions formed by side chain fragmentation of **3**. By accounting for these side chain fragments, it was possible to identify and assign the other peaks present in the MS/MS spectra.

During MS/MS analysis of peptides from HDAC8 that had been modified by **3**, fragmentation of probe **3** was observed at the sites indicated in Figure 7. These types of cleavages (e.g., y_{15}^{2+}−A) are indicated in the tandem mass spectra of modified HDAC8 peptides. There were a total of three fragment ions, *m*/*z* 689.1 (y_6^{1+}), 885.4 (b_{17}^{3+}), and 1190.4 (a_{15}^{2+}), that could be directly assigned to peptide backbone bond cleavages. Of those three, only the y_6^{1+} fragment corresponds to a region of the peptide not containing probe **3**. The remaining fragment ions were assigned to peptide backbone cleavages plus fragmentation of **3**. For three of the fragment ions, more than one type of fragment ion could be assigned. The overall HDAC8 sequence analyses ranged between 61% and 68% for the control HDAC8 samples and between 52% and 58% for modified HDAC8 protein samples.

To explore if there are more than one binding mode for HDAC ligands, we performed extensive MD simulations of

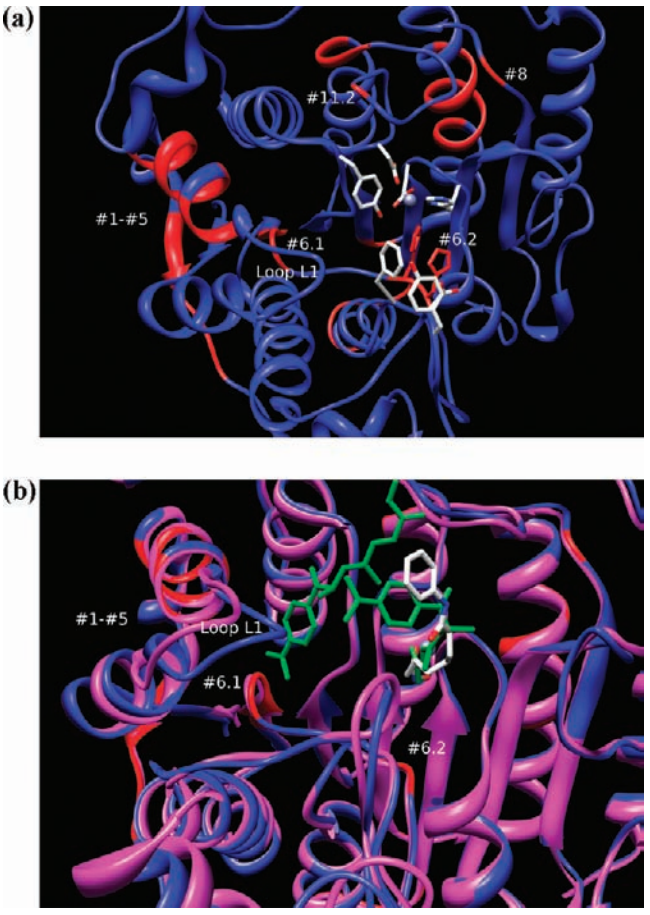

Figure 8. (a) Location of the peptides (red) modified with probe **3** mapped on HDAC8 PDB 1T69 (blue model). The numbers correspond to the entries in Table 3. The residues rendered as "sticks" correspond to the residues in the immediate proximity to SAHA in 1T69. (b) Same as for panel a. Overlay of HDAC8 1T69 (blue) and 1T64 (magenta). SAHA and TSA are rendered as "stick" models colored by atom types (SAHA) or green color (TSA).

ligands **1** and **3** bound to the HDAC8 and compared them with the outcomes of the photolabeling experiments described above for ligand **3**. The binding modes of the ligands are characterized by the conformation of the ligand inside the binding site and the resulting interactions between the SBG of the ligands and the various structural elements of the HDAC8 surface, i.e., R1−R3 and G1−G3 (Figure 2). To determine the binding modes available to the ligands, identical conformations sampled during the course of an MD simulation were identified using the matrix rmsd and confirmed with an analysis of the distances between the SBGs of SAHA and ligand **3** and representative amino acids in G1−G3 (Supporting Information).

In ligand **1** the binding mode 1 is represented by the areas in the rmsd matrix at 1, 5, 8.5−12, and 19.5−20 ns, the binding mode 2 at 2−4.5, 5.5, 13, 14−17, and 17.5−19.5 ns, and the binding mode 3 at 2, 5.5−8.5, 12, 13.5, and 17 ns. The rmsd matrix (Supporting Information) shows that ligand **1** changed from one binding mode to another multiple times during the course of the simulation, suggesting that they are the only ones available to the ligand. The fact that no new conformations were found after 2 ns in the remaining 18 ns of the simulation suggests that the conformational space of the bound ligand was fully sampled.

Characteristic interactions of each binding mode are determined by visual inspection of the conformation of the ligand

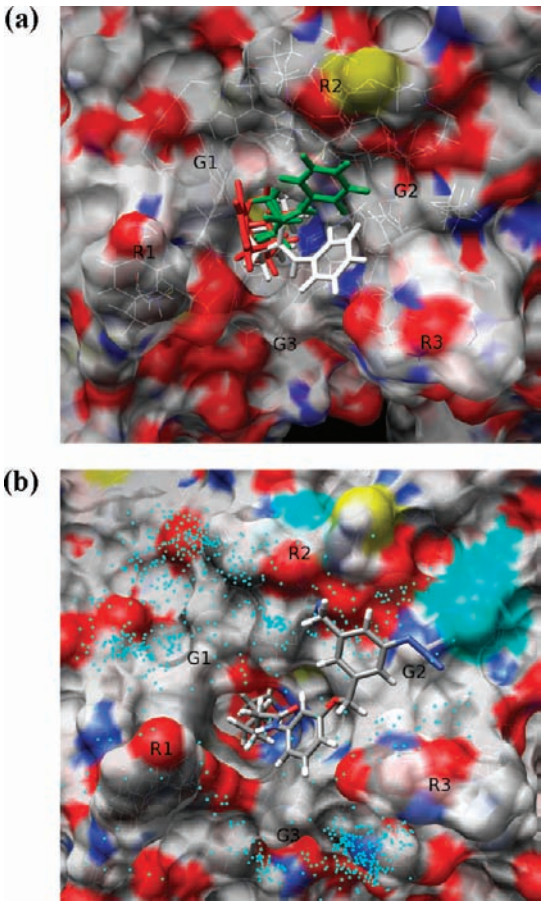

Figure 9. (a) Binding modes 1, 2, and 3 of SAHA indicated in white, green, and red, respectively. The surface is colored according to atom types using standard atom color convention. (b) The residues Asp233 and Asp272 modified by photoactivation of the probe **3** are marked by a cyan surface. The locations of the aromatic azide throughout the simulations are projected on the surface and are marked by cyan dots. Probe **3** is represented in a binding mode similar to the binding mode 2 observed for SAHA. G1−G3 and R1−R3 are grooves and ridges on the protein surface, respectively.

inside the binding site of HDAC8. In the first binding mode, the phenyl ring interacts with the area G2/R3 of the protein, whereas in the second binding mode the phenyl ring interacts with G2/R2 (Figure 9a). The third binding mode is similar to the binding mode of **1** observed in X-ray, as they are both characterized by strong electrostatic interaction between the amide group of **1** and Asp101 and weak interaction between the phenyl ring of **1** and the protein surface.

The analysis indicates that the second binding mode dominates, contributing approximately 35% of the total conformations. The first and third binding modes follow with an approximately equal weight, 22% and 21%, respectively. It is therefore expected that all the three major binding modes of SAHA collectively contribute to inhibition of HDAC8. Only the binding mode 3 is observed in the crystal structure PDB 1T69. The only difference between 1T69 and the binding mode 3 is the conformation of the amide group of SAHA. In 1T69 the carbonyl points toward the carboxylate of Asp101, one of the residues conserved in class I and II HDAC isoforms, whereas in the binding mode 3 the amide nitrogen of SAHA forms hydrogen bond with Asp101. Although recent crystal structures[44] of HDAC8 indicate the presence of a hydrogen bond between Asp101 and the amide nitrogen of the inhibitors, the protonation state of Asp101 remains a matter of debate.[45] Interestingly, with very few exceptions,[45] the majority of the HDAC X-rays contain an additional copy of the HDAC protein that not only shields the ligand from the solvent but also directly affects the binding of the ligand. It is therefore unclear how relevant the binding pose observed in the X-ray is to the actual pose of the cocrystallized ligands in the solution.

Similar exploration of all conformational space available to probe **3** would require running simulations for an unrealistically long time because of the increased number of degrees of freedom. To avoid it, we decided to use multiple binding poses of ligand **3** as starting conformations and perform several simulations simultaneously, a well accepted approach for exploring large conformational spaces. Probe **3** was docked to HDAC8, and 10 diverse binding poses were selected for further MD simulations. The total cumulated simulation time was more than 160 ns. The rmsd matrix of ligand **3** (Supporting Information) shows that, similar to ligand **1**, ligand **3** has three main binding modes. The binding mode 1 corresponds to 0−3, 28−32, 60−65, and 135−160 ns, the binding mode 2 to 20−28, 32−40, 50−60, 85−90, 120−135, and 165−168 ns, and the binding mode 3 to 3−20, 40−50, 65−85, 90−120, 120−135, 160−165, and 168−180 ns. As expected for a larger and more flexible molecule, the transition time from one binding mode to another is now longer compared to that observed for the binding modes of SAHA (Supporting Information). The binding modes 1, 2, and 3 have a weight of approximately 19%, 12%, and 46%, respectively, with the binding mode 3 now being predominant. Whereas these binding modes are not present in the same proportion as in ligand **1**, more than one major binding mode is available for ligand **3** as well.

Figure 9b shows the spatial distribution of the aromatic azide group throughout the simulations. The cyan dots represent all the locations occupied by the last nitrogen atom of the azide group of ligand **3**. The coordinates of this atom were taken from every frame of the simulation trajectory. The main density areas are located in the grooves and ridges G1/R2, R2, and G2/R2. The spatial distribution of the aromatic azide group during the simulation is consistent with the modification of the residues Asp233 and Asp272 observed by LC−MS/MS analysis, as it is mostly located in the vicinity of these residues. Importantly, the modification of these residues cannot be accomplished if the ligand exists only in a single binding pose, as the residues modified are located too far away from each other to be reacting with any single binding pose. The absence of modification corresponding to the azido group oriented toward G3 in pose 1 of probe **3** is consistent with its predominant solvent exposure and the fact that G3 is relatively deeper compared to G1 and G2. The sharper curvature of the surface near G3 prevents the remotely located aromatic azide moiety of probe **3** from making contact with the surface. These observations suggest that to improve the surface contact with G3, the introduction of a more flexible moiety between the linker and the SBG portions of the HDAC ligands may be necessary.

Conclusions

This is the first study where the binding poses available to the ligands in HDAC8 were determined experimentally by the BEProFL approach. The tagging of the probe **3** attached to HDAC8 with BT **4** resulted in a concentration dependent increase in biotinylation of the protein with the increase of the

concentration of probe **3** but not with probe **2** which lacks the second azido group. The selectivity of probe **3** for the active site of HDAC8 was demonstrated by blocking it with SAHA. Using the photoaffinity experiments, we show that probe **3** modifies the HDAC8 binding site at or near Asp^{233} and Asp^{272}, the interface areas between G1 and R2 and R2 and G2 that can only be reached if probe **3** adopts at least two different binding poses. The results of MD simulations are consistent with these observations. Sharper curvature of the HDAC8 protein surface in G3 explains the lack of covalent modifications in it. The modifications observed at His^{142}-His^{143} and Ile^{135}-Asn^{136}-Trp^{137}-Ser^{138} are likely attributed to the "upside-down" binding pose of probe **3** analogous to that of TSA. The other few modifications of the HDAC8 protein on the side opposite the binding site appear to be a result of aggregation with probe **3**. Although the three major poses available to SAHA and probe **3** are similar, they are not equally populated as determined by MD analysis. Overall, the findings demonstrated that multiple binding poses of the HDAC ligands are likely to contribute to the binding. Future studies are needed to learn how this observation can be used in HDAC drug design to improve the activity and selectivity of the ligands.

The study also highlights further directions in refinement of the BEProFL approach. Minimization of the fragmentation of the probe is highly desirable to facilitate the analysis of MS/MS data. The source of nonspecific tagging of the HDAC8 protein upon incubation with biotin tag **4** remains unclear, warranting further investigation.

The methodology supplies a unique power in analysis of the binding of ligands to their macromolecular targets by expanding the data typically obtained in the protein X-ray crystallography or providing an alternative tool when cocrystallization of the protein with the ligand of interest has failed. Most importantly, the binding poses determined by BEProFL are determined in solution and, thus, the captured "snapshots" reflect the dynamic nature of the ligand and its macromolecular target conformations. Extension of the BEProFL approach to study the binding poses of the ligands in cells is in progress in our laboratory. The approach has the potential not only to guide ligand optimization but also to become a new tool in disciplines such as molecular modeling, development, validation, and application of computer-aided drug design methods, especially those for rapid prediction of the protein−ligand interactions such as docking and scoring.

Experimental Procedures

General Synthetic Procedures. ^{1}H NMR and ^{13}C NMR spectra were recorded on Bruker spectrometer at 300/400 and 75/100 MHz, respectively, with TMS as an internal standard. Standard abbreviations indicating multiplicity were used as follows: s = singlet, bs = broad singlet, d = doublet, t = triplet, q = quadruplet, and m = multiplet. HRMS experiments were performed on Q-TOF-2TM (Micromass). TLC was performed with Merck $60F_{254}$ silica gel plates. Column chromatography was performed using Merck silica gel (40−60 mesh). Analytical HPLC was carried out on an Ace 5AQ column (100 mm × 4.6 mm) with a Shimadzu 10 VP series HPLC with a diode array detector with detection at λ = 254 nm. Method A consisted of the following: H_2O/MeCN (0.05% TFA), 70/30 to 0/100 in 25 min, flow rate of 1.3 mL/min. Method B consisted of the following: H_2O/MeCN (0.05% TFA), 90/10 to 0/100 in 25 min, flow rate of 1.3 mL/min. The purity of compounds determined by HPLC (methods A and B) was ≥95% for all the synthesized compounds.

7-[4-(3-Azidophenyl)thiazol-2-ylcarbamoyl]heptanoic Acid Methyl Ester (8). To a solution of **7** (0.350 g, 0.96 mmol) in a 9:1 mixture of acetic acid and water (15 mL) was added $NaNO_2$ (0.100 g, 1.45 mmol) at 0 °C, and the mixture was stirred for 5 min. To this was added NaN_3 (0.094 g, 1.45 mmol) at the same temperature, and stirring was continued for 30 min. To this was added saturated aqueous $NaHCO_3$ solution followed by $NaHCO_3$ powder until the mixture reached pH 7. The mixture was extracted with EtOAc and the combined organic extracts were washed with brine, dried (Na_2SO_4), filtered, and concentrated under reduced pressure to afford **8** (0.273 g, 73%). ^{1}H NMR (400 MHz, CD_3OD) δ 7.70 (d, J = 8.0 Hz, 1H), 7.66 (s, 1H), 7.44 (s, 1H), 7.41 (t, J = 7.6 Hz, 1H), 7.00 (dd, J = 7.6, 1.6 Hz, 1H), 3.65 (3H, s), 2.49 (t, J = 7.2 Hz, 2H), 2.34 (t, J = 7.6 Hz, 2H), 1.73 (t, J = 7.2 Hz, 2H), 1.64 (t, J = 6.8 Hz, 2H), 1.41(brs, 4H); ^{13}C NMR (100 MHz, DMSO-d_6) δ (ppm) 174.1, 170.2, 158.5, 148.5, 146.7, 136.0, 130.2, 122.5, 122.5, 117.5, 116.7, 108.7, 51.5, 36.2, 33.9, 28.6, 24.6, 24.5.

Octanedioic Acid [4-(3-Azidophenyl)thiazol-2-yl]amide Hydroxyamide (2). KOH (0.607 g, 10.85 mmol) was added at 40 °C for 10 min to a solution of hydroxylamine hydrochloride (0.753 g, 10.85 mmol) in MeOH. The reaction mixture was cooled to 0 °C and filtered. Compound **8** (0.210 g, 0.54 mmol) was added to the filtrate followed by KOH (36 mg, 0.65 mmol) at room temperature for 30 min and stirred for 4 h. The reaction mixture was extracted with EtOAc, and the organic layer was washed with a saturated NH_4Cl aqueous solution and brine, dried over Na_2SO_4, filtered, and concentrated. The crude solid was purified by preparative HPLC to give compound **2** (0.058 g, 28%). ^{1}H NMR (400 MHz, DMSO-d_6) δ (ppm) 12.25 (s, 1H), 10.32 (s, 1H), 8.64 (s, 1H), 7.74−7.62 (m, 3H), 7.05 (brs, 1H), 6.67 (brs, 1H), 2.49 (m, 2H), 1.93 (m. 2H), 1.26 (m, 2H), 1.10 (brs, 4H); ^{13}C NMR (100 MHz, DMSO-d_6) δ (ppm) 172.0, 169.5, 158.4, 148.0, 140.3, 136.5, 130.8, 122.8, 118.8, 116.3, 109.5, 35.2, 32.6, 25.4, 25.0; MS (ESI) m/z 389.1 $[M + H]^+$; HRMS (ESI) calculated for $[C_{17}H_{20}N_6O_3S_1 + H]^+$ 389.1390, found 389.1383.

7-(4-Benzyloxyphenylcarbamoyl)heptanoic Acid Methyl Ester (9). A stirring solution of 4-benzyloxyaniline hydrochloride (2.01 g, 10.10 mmol) and suberic acid monomethyl ester **5** (1.90 g, 10.10 mmol) in dry pyridine (20 mL) was cooled to −15 °C, and $POCl_3$ (1.2 mL, 13.13 mmol) was added dropwise over 30 min and stirred for 12 h at room temperature. The reaction mixture was diluted with EtOAc and washed thoroughly with saturated $KHSO_4$ solution and brine. The organic phase was dried over Na_2SO_4. The solvent was removed by rotary evaporation. The crude solid was washed with EtOAc to give compound **9** (2.27 g, 61%). ^{1}H NMR (400 MHz, CD_3OD): δ 7.42−7.26 (m, 7H), 7.11 (s, 1H), 6.93 (d, J = 7.8 Hz, 2H), 5.22 (s, 2H), 3.66 (s, 3H), 2.34−2.31 (m, 4H), 1.77−1.71 (m, 2H), 1.70−1.62 (m, 2H), 1.40−1.36 (m, 4H); ^{13}C NMR (100 MHz, CD_3OD) δ 174.2, 171.0, 155.5, 136.9, 131.3, 128.5, 127.9, 127.4, 121.6, 115.2, 70.3, 51.5, 37.4, 33.9, 28.7, 28.7, 25.4, 24.6.

7-(4-Hydroxyphenylcarbamoyl)heptanoic Acid Methyl Ester (10). A suspension of compound **9** (1.20 g, 3.24 mmol) and Pd/C (10 wt %, 0.120 g) in MeOH (20 mL) was reacted under hydrogen atmosphere at room temperature for 5 h. The catalyst was removed by filtration through a pad of Celite. The solvent was evaporated. The crude material was purified by flash chromatography (EtOAc/hexane, 2:1) to give compound **10** (0.742 g, 81%). ^{1}H NMR (400 MHz, CD_3OD) δ 7.31 (d, J = 8.8 Hz, 2H), 6.74 (d, J = 8.8 Hz, 2H), 3.65 (s, 3H), 2.34−2.31 (m, 4H), 1.71−1.61 (m, 4H), 1.39−1.34 (m, 4H); ^{13}C NMR (100 MHz, CD_3OD) δ 174.5, 172.8, 153.9, 130.2, 121.9, 114.7, 50.5, 36.2, 33.2, 28.4, 25.4, 24.2.

7-[4-(3-Azido-5-azidomethylbenzyloxy)phenylcarbamoyl]heptanoic Acid Methyl Ester (11). To a solution of **12** (0.250 g, 0.886 mmol) and 7-(4-hydroxyphenylcarbamoyl)heptanoic acid methyl ester **10** (0.247 g, 0.886 mmol) in dry acetone (8 mL) was added K_2CO_3 (0.367 g, 2.65 mmol) at ambient temperature, and the reaction mixture was stirred at the same temperature for 12 h. The

mixture was poured into water and extracted with EtOAc. The organic layer was washed with water three times, dried over Na_2SO_4, and evaporated in vacuo. The residue was purified by flash chromatography (EtOAc/hexane, 2:1) to afford **11** (0.272 g, 66%). ^{1}H NMR (400 MHz, $CDCl_3$): δ 7.43 (d, J = 8.8 Hz, 2H), 7.15 (s, 1H), 7.11 (s, 1H), 7.08 (s, 1H), 6.92 (d, J = 9.2 Hz, 2H), 5.04 (s, 1H), 4.37 (s, 1H), 3.69 (s, 3H), 2.36−2.31 (m, 4H), 1.74 (t, J = 8.0 Hz, 2H), 1.65 (t, J = 7.2 Hz, 2H), 1.40 (brs, 4H); ^{13}C NMR (100 MHz, $CDCl_3$) δ 174.2, 171.0155.0, 141.0, 139.8, 137.8, 131.6, 124.2, 123.1, 121.6, 119.1, 118.7, 117.9, 117.5, 115.1, 69.3, 54.1, 51.4, 37.4, 33.9, 28.6, 25.3, 24.6.

Octanedioic Acid [4-(3-Azido-5-azidomethylbenzyloxy)phenyl]-amide Hydroxyamide (3). KOH (0.481 g, 8.60 mmol) was added at 40 °C for 10 min to a solution of hydroxylamine hydrochloride (0.597 g, 8.60 mmol) in MeOH. The reaction mixture was cooled to 0 °C and filtered. Compound **11** (0.200 g, 0.43 mmol) was added to the filtrate followed by KOH (28 mg, 0.51 mmol) at room temperature for 30 min and stirred for 4 h. The reaction mixture was extracted with EtOAc, and the organic layer was washed with a saturated NH_4Cl aqueous solution and brine, dried over Na_2SO_4, filtered, and concentrated. The crude solid was purified by preparative HPLC to give compound **3** (0.080 g, 40%). ^{1}H NMR (400 MHz, DMSO-d_6) δ 10.32 (s, 1H), 9.72 (s, 1H), 8.65 (s, 1H), 7.48 (d, J = 7.3 Hz, 2H), 7.26 (s, 1H), 7.16 (s, 1H), 7.09 (s, 1H), 6.94 (d, J = 8.6 Hz, 2H), 5.09 (s, 1H), 4.50 (s, 1H), 2.24 (t, J = 7.2 Hz, 2H), 1.93 (t, J = 7.0 Hz, 2H), 1.55−1.46 (m, 4H), 1.26 (brs, 4H); ^{13}C NMR (100 MHz, DMSO-d_6) δ 171.1, 169.52, 154.19, 140.48, 140.38, 138.56, 133.37, 124.36, 120.96, 118.61, 118.0, 115.2, 68.9, 53.3, 36.6, 32.6, 28.8, 25.52, 25.47; MS (ESI) m/z 467.2 $[M + H]^+$; HRMS (ESI) calculated for $[C_{22}H_{26}N_8O_4 + H]^+$ 467.2140, found 467.2149.

Biological Materials. The HDAC8 fluorescent assay kit and the human recombinant HDAC8 protein were purchased from Biomol International (Plymouth Meeting, PA). Cell culture media MEM/EBSS, Ham's F12, fetal bovine serum (FBS), and nonessential amino acids (NEAA) were purchased from Hyclone (Logan, UT). Cell culture dishes were purchased from BD Falcon (BD Biosciences, San Jose, CA). The primary anti-HDAC8 antibody was from Santa Cruz (Santa Cruz, CA) respectively. The antirabbit secondary antibody conjugated to horseradish peroxidase (HRP) was from GE (Piscataway, NJ). Streptavidin and the colorimetric HRP substrate *o*-phenylenediamine (OPD) were from Pierce (Rockford, IL) and the 96-well plates from Nunc (Rochester, NY). Tris(2-carboxyethyl)phosphine) (TCEP) was from (Alfa Aesar chemicals, Ward Hill, MA). $CuSO_4$, dimethyl sulfoxide (DMSO), tris((1-benzyl-1*H*-1,2,3-triazol-4-yl)methyl)amine (TBTA), and all other chemicals were purchased from Sigma (St. Louis, MO) if not stated otherwise.

HDAC Activity Assay. The assay proceeded through a simple two-step procedure that can be carried out in half-volume microtitration plates. The in vitro fluoro HDAC assay was performed in HDAC assay buffer (25 mM Tris (pH 8.0), 137 mM NaCl, 2.7 mM KCl, 1 mM $MgCl_2$) supplemented with 0.5 mg/mL BSA. After 30 min, an amount of 50 μL of developer supplemented with 5 μM trichostatin A to inactivate the enzyme was added. The fluorescence experiments were conducted at λ_{excit} = 360 nm and λ_{emis} = 460 nm using a POLARStar Optima microtitration plate reader (BMG Labtech, Durham, NC). The IC_{50} values were determined using the GraphPad Prism 5 software. K_I values were calculated using the Cheng−Prusoff equation[46] and a K_m for the substrate equal to 222 μM for HDAC8.

Visualization of Probe 3 Attached to HDAC 8 Using Biotinylated Tag 4. Purified recombinant human HDAC8 (0.5 μg in 5 μL of assay buffer) was incubated with various concentrations of **2**, **3**, and SAHA for 3 h in the dark, after which the formation of a covalent bond between the azide group present in the ligand and reactive side chains of the HDAC was initiated by UV irradiation (λ = 254 nm) for 3 × 1 min with 1 min rest. Then "click chemistry" was used to attach BT **4** to probe **3** attached covalently to the protein. The biotin tag **4** was added to all the tubes at a final concentration of 50 μM, and the chemical reaction was initiated by addition of TCEP (0.5 mM final concentration), TBTA (0.1 mM), and $CuSO_4$ (1 mM). After 90 min of incubation at room temperature, protein samples were analyzed by SDS−PAGE and Western blot using an antibiotin primary antibody, streptavidin conjugated to horseradish peroxidase (Pierce (Rockford, IL), and ECL (Pierce (Rockford, IL). The membranes were then stripped in 0.2 M glycine, pH 2.6 for 10 min, and then in 0.2 M glycine, pH 2.3 for another 10 min, before being reblocked and redecorated with an anti-HDAC primary antibody and an antirabbit-HRP secondary antibody.

Western Blotting. Western blot was performed using 10 μg of total protein from cell lysate or 0.5 μg of purified protein with 5× loading buffer containing 10% SDS, 0.05% bromophenol blue, 50% glycerol, and β-mercaptoethanol. Protein samples were boiled for 5 min and allowed to cool before loading on a denaturing 10% polyacrylamide gel electrophoresis (SDS−PAGE). After electrophoresis, protein was transferred to a polyvinylidiene difluoride membrane (Imobilon-Millipore, Bedford, MA). The membrane was incubated for 1 h with 1% albumin fraction V (USB, OH) and washed three times with 1× phosphate buffer saline supplemented with 0.05% of Tween-20 (PBS-T). The membrane was then incubated with an anti-HDAC8 antibody (1:3000) for 2 h under room temperature with slight agitation. After three washes in PBS-T, the membranes were incubated with a secondary antibody antirabbit-HRP for 1 h at room temperature. The signals were detected using the enhanced chemiluminescence (ECL) kit from Pierce (Pierce Biotechnology, Rockford, IL). Densitometry scanning of the films was performed using the ImageJ software provided by NIH.[47,48] Data obtained from at least three independent experiments are presented as the mean of the relative intensity of the biotinylated bands over the total immunoreactive HDAC bands ± standard deviation (SD).

MALDI-ToF MS Analysis of Intact HDAC8 Protein. The samples were purified and concentrated using Centricon 10 000 molecular weight cutoff filter filters (Millipore) according to the manufacturer's instructions. Prior to use, the filters were washed three times with 400 μL of 50 mM ammonium bicarbonate, pH 7.8. Aliquots of 25 μL of each HDAC8 sample were then diluted to a total volume of 250 μL with the ammonium bicarbonate buffer and applied to the prerinsed filters. The samples were centrifuged at 13500*g* at 4 °C for 60 min. After centrifugation, the filter was transferred to a second 1.5 mL microcentrifuge tube inverted and centrifuged at 1000*g* for 6 min. The recovered protein (approximately 3−5 μL) was mixed with 3 μL of MALDI matrix and spotted on a MALDI plate for analysis. The MALDI matrix was saturated with sinapinic acid in 50:50 (v/v) H_2O/ACN + 0.1% TFA. Positive ion MALDI mass spectra were acquired using an Applied Biosystems Voyager DE Pro MALDI-ToF MS.

Tryptic Digestion of HDAC8 and Modified HDAC8. HDAC8 (∼10 μg) was incubated with 5 equiv of probe **3**, irradiated with UV light to activate the probe, and tagged with BT **4**. Next, the modified protein was purified using avidin−agarose chromatography. Unmodified HDAC8 was used as a negative control. Each sample of modified or unmodified HDAC8 was diluted to a final volume of 100 μL with an aqueous buffer containing 50 mM ammonium bicarbonate (AMBIC) and 1 mM TCEP (pH 7.8). Prior to digestion, all samples were tested to ensure that their pH was between 7.0 and 8.0. Control samples containing 10 μg of HDAC8 were treated with 200 ng of sequence grade modified trypsin (Promega), while the modified HDAC8 samples (≤10 μg each) were treated with 100 ng of trypsin. Digestions were carried out for 15 h and then analyzed using LC−MS/MS.

1-D LC−MS/MS Analysis of Tryptic Digests. Tryptic digests were analyzed using an Ultimate 3000 capillary HPLC system (Dionex) interfaced with a LTQ-FT hybrid linear ion trap FT ICR mass spectrometer (Thermo-Fisher Scientific) that was operated using positive ion nanoelectrospray with data-dependent MS/MS.

The resolving power of the FT ICR mass spectrometer was ~100 000. Charge state screening was used to exclude singly charged ions. Samples were diluted to a concentration of ~0.1 pmol/μL of total protein using 50 mM AMBIC. The LC−MS/MS injection volume was 5 μL. The mobile phases consisted of A (95/5 (v/v) H_2O/CH_3CN + 0.1% formic acid) and B (5/95 (v/v) H_2O/CH_3CN + 0.1% formic acid). The trapping column (0.3 mm i.d. × 5 mm Dionex C_{18} PepMap column) was operated at a flow rate of 15 μL/min using 100% solvent A during sample loading. The analytical column (75 μm × 150 mm Agilent Zorbax 300-SB C_{18} column) was used to separate the peptide digests of HDAC, and modified HDAC was operated at a flow rate of 190 nL/min and was equipped with a PEEK sleeve fitting containing a 75 μm i.d. pulled fused silica nanoelectrospray emitter (New Objective) with a tip i.d. of 15 μm. An 85 min linear gradient was used from 3% to 95% solvent B followed by a 10 min re-equilibration prior to the next analysis. Following LC−MS/MS analysis, the data were searched using SEQUEST (Bio Works 3.2) proteomics software.

Graphics. The protein surface in Figure 2 is rendered in Vida3.0.[49] The images in Figures 8 and 9 were rendered in Chimera.[50]

Molecular Dynamics Simulations. Molecular dynamics simulations were performed using the GROMACS software package (version 3.3.1),[29−32] the Amber03 force field[33] and the general Amber force field (GAFF)[35,36] together with AM1BCC charges.[38,39] The structure of HDAC8 and the starting conformation of SAHA were taken from the X-ray structure of HDAC8 forming a complex with SAHA (PDB structure 1T69). Since no crystal structure is available for ligand **3**, the starting structures were obtained from the docking of ligand **3** to HDAC8 using the docking software Gold 3.2.[40] TIP3P explicit solvent was used.[51] All simulations were run in a dodecahedral box containing approximately 9100 water molecules. The bonds of the protein and ligands were constrained using the LINCS algorithm,[52] while the bonds and angle of the water molecules were constrained using the SETTLE algorithm.[53] A time step of 2 fs was used for integrating the equations of motion. The system was simulated in an NTP ensemble at a fixed temperature of 300 K and a fixed pressure of 1 bar. Temperature was kept constant using a Berendsen thermostat[54] with a coupling time of 0.1 ps, and pressure was controlled by a weak coupling to a reference pressure[55] with a coupling time of 1 ps and an isothermal compressibility of 4.6×10^{-5} bar^{-1}. Long-range Coulombic interactions were evaluated using the particle mesh Ewald (PME) algorithm[56] with an interpolation order of 4 and Fourier spacing of 1.2 Å. The system was energy minimized and then equilibrated for 200 ps in total. Finally the simulations were run for 20 ns each.

Root mean square deviation (rmsd) matrices of the ligands were built for each simulation trajectory by calculating the rmsd of each structure of the ligand with all other structures of the same ligand in the trajectory. All protein structures in the trajectory were aligned using the least-squares fitting of the protein backbone. The final rmsd calculations of the ligands were performed on their heavy atoms using the atoms corresponding to the scaffold of SAHA.

Any two conformations of a ligand were considered different if their rmsd values were more than 2 Å. By use of this cutoff value as a similarity criterion for the rmsd between two conformations, identical conformations were identified and represented by a white point on the matrix, whereas different conformations were represented by a black point. As a consequence, a white block on the matrix diagonal represents a group of identical conformations and a white block off diagonal indicates that the corresponding two groups on the diagonal contain identical conformations. By use of this technique, different sets of identical conformations corresponding to the different binding modes of the ligand can be readily identified. The (rmsd) matrices of the ensemble of conformations sampled for ligands **1** and **3** are shown in the Supporting Information.

The binding modes of **1** and **3** determined using the rmsd matrix were confirmed by monitoring characteristic distances between the interacting groups. The residues were selected in such a way that a distance less than 5 Å between the center of mass of the phenyl ring of **1** and Phe208 would indicate that ligand **1** is in G2/R3. Similarly a distance less than 5 Å between the center of mass of the phenyl ring of **1** and the center of mass of Met274 would be indicative of ligand **1** in G2/R2, a distance less than 5 Å between the amide NH of the SBG and the center of mass of Asp101 would be indicative of ligand 1 near R1. The same distance characteristics of the three binding modes of **1** have been monitored for **3**. The results of this analysis are shown in the Supporting Information.

Acknowledgment. This study was in part funded by the Breast Cancer Congressionally Directed Research Program of Department of Defense Idea Award BC051554 and by the National Cancer Institute/NIH Grant 1R01 CA131970-01A1. We also thank Chicago Biomedical Consortium and Searle family for the support of FT ICR MS and the National Center for Research Resources/NIH Grant 1S10 RR14686 for the MALDI ToF mass spectrometer. Molecular graphics images were produced using the UCSF Chimera package from the Resource for Biocomputing, Visualization, and Informatics at the University of California, San Francisco (supported by NIH Grant P41 RR-01081) and OpenEye Scientific Software, Santa Fe, NM.

Supporting Information Available: The rmsd matrixes and distance analysis figures and synthetic procedures for BT **4**. This material is available free of charge via the Internet at http://pubs.acs.org.

References

(1) Korner, M.; Tibes, U. Histone deacetylase inhibitors: a novel class of anti-cancer agents on its way to the market. *Prog. Med. Chem.* **2008**, *46*, 205–280.
(2) Marks, P. A.; Richon, V. M.; Rifkind, R. A. Histone deacetylase inhibitors: inducers of differentiation or apoptosis of transformed cells. *J. Natl. Cancer Inst.* **2000**, *92*, 1210–1216.
(3) de Ruijter, A. J.; van Gennip, A. H.; Caron, H. N.; Kemp, S.; van Kuilenburg, A. B. Histone deacetylases (HDACs): characterization of the classical HDAC family. *Biochem. J.* **2003**, *370*, 737–749.
(4) Hahnen, E.; Hauke, J.; Trankle, C.; Eyupoglu, I. Y.; Wirth, B.; Blumcke, I. Histone deacetylase inhibitors: possible implications for neurodegenerative disorders. *Expert Opin. Invest. Drugs* **2008**, *17*, 169–184.
(5) Wang, D. F.; Helquist, P.; Wiech, N. L.; Wiest, O. Toward selective histone deacetylase inhibitor design: homology modeling, docking studies, and molecular dynamics simulations of human class I histone deacetylases. *J. Med. Chem.* **2005**, *48*, 6936–6947.
(6) Nielsen, P. E. *Photochemical Probes in Biochemistry*; Kluwer Academic Publishers: Dordrecht, The Netherlands, 1989; Vol. 272.
(7) Rajagopalan, K.; Watt, D. S.; Haley, B. E. Orientation of GTP and ADP within their respective binding sites in glutamate dehydrogenase. *Eur. J. Biochem.* **1999**, *265*, 564–571.
(8) Olcott, M. C.; Bradley, M. L.; Haley, B. E. Photoaffinity labeling of creatine kinase with 2-azido- and 8-azidoadenosine triphosphate: identification of two peptides from the ATP-binding domain. *Biochemistry* **1994**, *33*, 11935–11941.
(9) Speers, A. E.; Adam, G. C.; Cravatt, B. F. Activity-based protein profiling in vivo using a copper(I)-catalyzed azide-alkyne [3 + 2] cycloaddition. *J. Am. Chem. Soc.* **2003**, *125*, 4686–4687.
(10) Adam, G. C.; Burbaum, J.; Kozarich, J. W.; Patricelli, M. P.; Cravatt, B. F. Mapping enzyme active sites in complex proteomes. *J. Am. Chem. Soc.* **2004**, *126*, 1363–1368.
(11) Sieber, S. A.; Mondala, T. S.; Head, S. R.; Cravatt, B. F. Microarray platform for profiling enzyme activities in complex proteomes. *J. Am. Chem. Soc.* **2004**, *126*, 15640–15641.
(12) Speers, A. E.; Cravatt, B. F. A tandem orthogonal proteolysis strategy for high-content chemical proteomics. *J. Am. Chem. Soc.* **2005**, *127*, 10018–10019.
(13) Hanson, S. R.; Hsu, T. L.; Weerapana, E.; Kishikawa, K.; Simon, G. M.; Cravatt, B. F.; Wong, C. H. Tailored glycoproteomics and

glycan site mapping using saccharide-selective bioorthogonal probes. *J. Am. Chem. Soc.* **2007**, *129*, 7266–7267.
(14) Li, W.; Blankman, J. L.; Cravatt, B. F. A functional proteomic strategy to discover inhibitors for uncharacterized hydrolases. *J. Am. Chem. Soc.* **2007**, *129*, 9594–9595.
(15) Salisbury, C. M.; Cravatt, B. F. Activity-based probes for proteomic profiling of histone deacetylase complexes. *Proc. Natl. Acad. Sci. U.S.A.* **2007**, *104*, 1171–1176.
(16) Hosoya, T.; Hiramatsu, T.; Ikemoto, T.; Nakanishi, M.; Aoyama, H.; Hosoya, A.; Iwata, T.; Maruyama, K.; Endo, M.; Suzuki, M. Novel bifunctional probe for radioisotope-free photoaffinity labeling: compact structure comprised of photospecific ligand ligation and detectable tag anchoring units. *Org. Biomol. Chem.* **2004**, *2*, 637–641.
(17) Sun, P.; Wang, G. X.; Furuta, K.; Suzuki, M. Synthesis of a bis-azido analogue of acromelic acid for radioisotope-free photoaffinity labeling and biochemical studies. *Bioorg. Med. Chem. Lett.* **2006**, *16*, 2433–2436.
(18) Hosoya, T.; Hiramatsu, T.; Ikemoto, T.; Aoyama, H.; Ohmae, T.; Endo, M.; Suzuki, M. Design of dantrolene-derived probes for radioisotope-free photoaffinity labeling of proteins involved in the physiological Ca^{2+} release from sarcoplasmic reticulum of skeletal muscle. *Bioorg. Med. Chem. Lett.* **2005**, *15*, 1289–1294.
(19) Saxon, E.; Armstrong, J. I.; Bertozzi, C. R. A "traceless" Staudinger ligation for the chemoselective synthesis of amide bonds. *Org. Lett.* **2000**, *2*, 2141–2143.
(20) Saxon, E.; Bertozzi, C. R. Cell surface engineering by a modified Staudinger reaction. *Science* **2000**, *287*, 2007–2010.
(21) Kiick, K. L.; Saxon, E.; Tirrell, D. A.; Bertozzi, C. R. Incorporation of azides into recombinant proteins for chemoselective modification by the Staudinger ligation. *Proc. Natl. Acad. Sci. U.S.A.* **2002**, *99* (1), 19–24.
(22) Saxon, E.; Luchansky, S. J.; Hang, H. C.; Yu, C.; Lee, S. C.; Bertozzi, C. R. Investigating cellular metabolism of synthetic azidosugars with the Staudinger ligation. *J. Am. Chem. Soc.* **2002**, *124*, 14893–14902.
(23) Vocadlo, D. J.; Hang, H. C.; Kim, E. J.; Hanover, J. A.; Bertozzi, C. R. A chemical approach for identifying O-GlcNAc-modified proteins in cells. *Proc. Natl. Acad. Sci. U.S.A.* **2003**, *100*, 9116–9121.
(24) Vocadlo, D. J.; Bertozzi, C. R. A strategy for functional proteomic analysis of glycosidase activity from cell lysates. *Angew. Chem., Int. Ed.* **2004**, *43*, 5338–5342.
(25) Al-Mawsawi, L. Q.; Fikkert, V.; Dayam, R.; Witvrouw, M.; Burke, T. R., Jr.; Borchers, C. H.; Neamati, N. Discovery of a small-molecule HIV-1 integrase inhibitor-binding site. *Proc. Natl. Acad. Sci. U.S.A.* **2006**, *103*, 10080–10085.
(26) Kozikowski, A. P.; Chen, Y.; Gaysin, A.; Chen, B.; D'Annibale, M. A.; Suto, C. M.; Langley, B. C. Functional differences in epigenetic modulators-superiority of mercaptoacetamide based-HDAC inhibitors relative to hydroxamates in cortical neuron neuroprotection studies. *J. Med. Chem.* **2007**, *50*, 3054–3061.
(27) Hosoya, T.; Hiramatsu, T.; Ikemoto, T.; Aoyama, H.; Ohmae, T.; Endo, M.; Suzuki, M. Design of dantrolene-derived probes for radioisotope-free photoaffinity labeling of proteins involved in the physiological Ca^{2+} release from sarcoplasmic reticulum of skeletal muscle. *Bioorg. Med. Chem. Lett.* **2005**, *15*, 1289–1294.
(28) Lin, P. C.; Ueng, S. H.; Yu, S. C.; Jan, M. D.; Adak, A. K.; Yu, C. C.; Lin, C. C. Surface modification of magnetic nanoparticle via Cu(I)-catalyzed alkyne-azide [2 + 3] cycloaddition. *Org. Lett.* **2007**, *9*, 2131–2134.
(29) Berendsen, H. J. C.; van der Spoel, D.; van Drunen, R. GROMACS: a message-passing parallel molecular dynamics implementation. *Comput. Phys. Commun.* **1995**, *91*, 43–56.
(30) Lindal, E.; Hess, B.; van der Spoel, D. GROMACS 3.0: a package for molecular simulation and trajectory analysis. *J. Mol. Model.* **2001**, *7*, 306–317.
(31) Van Der Spoel, D.; Van Buuren, A. R.; Apol, E.; Meulenhoff, P. J.; Tieleman, D. P.; Sijbers, A. L. T. M.; Hess, B.; Feenstra, K. A.; Lindahl, E.; Drunen, R. v.; Berendsen, H. J. C. *GROMACS User Manual*, version 3.0; Nijenborgh 4, 9747 AG: Groningen, The Netherlands, 2001; http://www.gromacs.org.
(32) Van Der Spoel, D.; Lindahl, E.; Hess, B.; Groenhof, G.; Mark, A. E. GROMACS: fast, flexible and free. *J. Comput. Chem.* **2005**, *26*, 1701–1718.
(33) Cornell, W. D.; Cieplak, P.; Barly, C. I.; Gould, I. R.; Merz, K. M.; Ferguson, D. M.; Spellmeyer, D. C.; Fox, T.; Caldwell, J. W.; Kollman, P. A. A second generation force field for the simulation of proteins, nucleic acids, and organic molecules. *J. Am. Chem. Soc.* **1995**, *117*, 5179–5197.
(34) Sorin, E. J.; Rhee, Y. M.; Pande, V. S. Does water play a structural role in the folding of small nucleic acids? *Biophys. J.* **2005**, *88*, 2516–2524.
(35) Wang, J.; Wolf, R. M.; Caldwell, J. W.; Kollman, P. A.; Case, D. A. Development and testing of a general Amber force field. *J. Comput. Chem.* **2004**, *25*, 1157–1174.
(36) Wang, J.; Wang, W.; Kollman, P. A.; Case, D. A. Automatic atom type and bond type perception in molecular mechanical calculations. *J. Mol. Graph. Modell.* **2006**, *25*, 247–260.
(37) Pieffet, G.; Petukhov, P. A. Parameterization of aromatic azido groups: application as photoaffinity probes in molecular dynamics studies. *J. Mol. Model.* **2009**, *15*, 1291–1297.
(38) Jakalian, A.; Bush, B. L.; Jack, D. B.; Bayly, C. I. Fast, efficient generation of high-quality atomic charges. AM1-BCC model: I: Method. *J. Comput. Chem.* **2000**, *21*, 132–146.
(39) Jakalian, A.; Jack, D. B.; Bayly, C. I. Fast, efficient generation of high-quality atomic charges. AM1-BCC model: II: Parameterization and validation. *J. Comput. Chem.* **2002**, *23*, 1623–1641.
(40) Jones, G.; Willett, P.; Glen, R. C.; Leach, A. R.; Taylor, R. Development and validation of a genetic algorithm for flexible docking. *J. Mol. Biol.* **1997**, *267*, 727–748.
(41) Suzuki, T.; Kouketsu, A.; Matsuura, A.; Kohara, A.; Ninomiya, S.; Kohda, K.; Miyata, N. Thiol-based SAHA analogues as potent histone deacetylase inhibitors. *Bioorg. Med. Chem. Lett.* **2004**, *14*, 3313–3317.
(42) Chen, Y.; Lopez-Sanchez, M.; Savoy, D. N.; Billadeau, D. D.; Dow, G. S.; Kozikowski, A. P. A series of potent and selective, triazolylphenyl-based histone deacetylases inhibitors with activity against pancreatic cancer cells and *Plasmodium falciparum*. *J. Med. Chem.* **2008**, *51*, 3437–3448.
(43) Somoza, J. R.; Skene, R. J.; Katz, B. A.; Mol, C.; Ho, J. D.; Jennings, A. J.; Luong, C.; Arvai, A.; Buggy, J. J.; Chi, E.; Tang, J.; Sang, B. C.; Verner, E.; Wynands, R.; Leahy, E. M.; Dougan, D. R.; Snell, G.; Navre, M.; Knuth, M. W.; Swanson, R. V.; McRee, D. E.; Tari, L. W. Structural snapshots of human HDAC8 provide insights into the class I histone deacetylases. *Structure* (*Cambridge, MA, U. S.*) **2004**, *12*, 1325–1334.
(44) Vannini, A.; Volpari, C.; Gallinari, P.; Jones, P.; Mattu, M.; Carfi, A.; De Francesco, R.; Steinkuhler, C.; Di Marco, S. Substrate binding to histone deacetylases as shown by the crystal structure of the HDAC8−substrate complex. *EMBO Rep.* **2007**, *8*, 879–884.
(45) Dowling, D. P.; Gantt, S. L.; Gattis, S. G.; Fierke, C. A.; Christianson, D. W. Structural studies of human histone deacetylase 8 and its site-specific variants complexed with substrate and inhibitors. *Biochemistry* **2008**, *47*, 13554–13563.
(46) Cheng, Y. C.; Prusoff, W. H. Relationship between the inhibition constant (K_i) and the concentration of inhibitor which causes 50% inhibition (IC_{50}) of an enzymatic reaction. *Biochem. Pharmacol.* **1973**, *22*, 3099–3108.
(47) Girish, V.; Vijayalakshmi, A. Affordable image analysis using NIH Image/ImageJ. *Indian J. Cancer* **2004**, *41*, 47.
(48) Eliceiri, K. W.; Rueden, C. Tools for visualizing multidimensional images from living specimens. *Photochem. Photobiol.* **2005**, *81*, 1116–1122.
(49) *Vida*, version 3.0; Openeye Scientific Software LLC: Santa Fe, NM, 2008.
(50) Pettersen, E. F.; Goddard, T. D.; Huang, C. C.; Couch, G. S.; Greenblatt, D. M.; Meng, E. C.; Ferrin, T. E. UCSF Chimera, a visualization system for exploratory research and analysis. *J. Comput. Chem.* **2004**, *25*, 1605–1612.
(51) Jorgensen, W. L.; Chandrasekhar, J.; Madura, J. D.; Impey, R. W.; Klein, M. L. Comparison of simple potential functions for simulating liquid water. *J. Chem. Phys.* **1983**, *79*, 926–935.
(52) Hess, B.; Bekker, H.; Berendsen, H. J. C.; Fraaije, J. G. E. M. LINCS: a linear constraint solver for molecular simulations. *J. Comput. Chem.* **1997**, *18*, 1463–1472.
(53) Miyamoto, S.; Kollman, P. A. SETTLE: an analytical version of the SHAKE and RATTLE algorithms for rigid water models. *J. Comput. Chem.* **1992**, *13*, 952–962.
(54) Berendsen, H. J. C.; Postma, J. P. M.; van Gunsteren, W. F.; DiNola, A.; Haak, J. R. Molecular dynamics with coupling to an external bath. *J. Chem. Phys.* **1984**, *81*, 3684–3690.
(55) *Molecular-Dynamics Simulations of Statistical-Mechanical Systems*; Hoover, W. G., Ed.; North-Holland: Amsterdam, 1986.
(56) Darden, T.; York, D.; Pedersen, L. Particle mesh Ewald: an *N*-log(*N*) method for Ewald sums in large systems. *J. Chem. Phys.* **1993**, *98*, 10089–10092.